Mid-Wave Infrared 3D Integral Imaging at Long Range

Daniel LeMaster, Barry Karch, and Bahram Javidi, *Fellow, IEEE*

***Abstract*—Integral imaging is an established method for passive three-dimensional (3D) image formation, visualization, and ranging. The applications of integral imaging include significantly improved scene segmentation and the ability to visualize occluded objects. Past demonstrations of this technique have been mainly conducted over short ranges achievable in the laboratory. In this paper, we demonstrate 3D computational integral imaging for ranges out to 2 km using multiple looks from a single moving mid-wave infrared (MWIR) imager. We also demonstrate 3D visualization of occluded objects at ranges over 200 m. To our knowledge, this paper is the first such demonstration at these ranges and the first example of this technique using a mid wave IR imaging system. In addition to presenting results, we also outline our new approach for overcoming the technical challenges unique to long range applications of integral imaging. Future applications of long range 3D integral imaging may include aerospace, search and rescue, satellite 3D imaging, etc.**

***Index Terms*—Computational integral imaging (CII), infrared imaging, passive 3-D imaging.**

I. Introduction

THERE is great interest in three-dimensional (3D) imaging for applications such as 3D TV, biomedical imaging, entertainment, computer vision, robotics, and defense [1]–[18]. Integral imaging [7] is a 3D passive sensing and visualization technique that can be applied to these problems. In this method, multiple 2D images (elemental images) with different perspectives are captured through a lens or camera array and then visualized through optical or computer processing. For 3D optical display, this approach provides full parallax (horizontal and vertical), continuous viewing points, and no visual fatigue. In addition, it does not require special glasses to observe the 3D images. Therefore, it is most likely to be the next generation 3D imaging system. However, there are some challenges to be solved including low viewing resolution, narrow viewing angle, and limited depth range. Potential solutions to these problems have been reported [8]–[13].

In an integral imaging system, there are two separate procedures for image capture (pickup) and reconstruction of 3D objects. In the pickup stage, multiple 2D elemental images are recorded through the lens or camera array. Each lens encodes 3D object information into 2D elemental images. Thus, many 2D elemental images with different perspectives record the direction and intensity of rays coming from the 3D object through the lens (or camera) array, as depicted in Fig. 1(a).

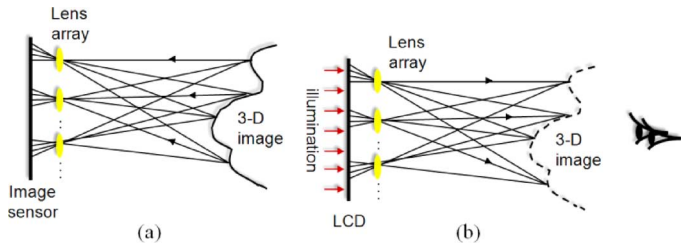

Fig. 1. Principle of integral imaging. (a) Image pickup. (b) 3D optical display.

For optical reconstruction of the 3D scene, a 2D display device such as a liquid crystal display (LCD) projects the elemental images onto the focal plane of the display lens array as shown in Fig. 1(b). Each 2D elemental image is optically transmitted by its corresponding lens back into 3D space. The overlap of all transmitted elemental images creates local light distributions similar to the original object of interest. As a result, an observer can see a real 3D image with full parallax and continuous viewing points.

In this paper, we use synthetic aperture integral imaging and computational reconstruction to demonstrate 3D visualization of objects and 3D imaging through obscuration over very long distances compared to anything else published to date. We demonstrate 3D integral imaging at ranges up to 2 km. Additionally, we demonstrate that this technique readily transfers to infrared imaging sensors in the 3–5 μm [mid-wave infrared (MWIR)] transmission band. In Section II, we describe our methods for data collection in the pick-up stage of integral imaging. Sections III and IV describe our experiments in obscuration penetration and passive ranging. The paper concludes with a summary of this work in Section V.

II. Synthetic Aperture Integral Imaging and Computational Reconstruction

We begin by presenting a short overview of computational reconstruction of integral imaging. The 3D reconstruction of scene is achieved numerically by simulating the optical back-projection of the multiple 2D images in computers. Intrinsically, the resolution of each elemental image is limited by three parameters: pixel size, lenslet point spread function, and lenslet depth of focus. However, integral imaging can also be performed in either a synthetic aperture mode or with an array of image sensors in which well corrected optics record

Manuscript received August 17, 2012; revised December 31, 2012; accepted February 05, 2013. Date of publication March 07, 2013; date of current version July 10, 2013.

D. LeMaster and B. Karch are with the Air Force Research Laboratory, AFRL/RYMT, 2241 Avionics Circle, Bldg 620, Wright Patterson Air Force Base, OH 45433 USA (e-mail: daniel.lemaster@wpafb.af.mil; Barry.Karch@wpafb.af.mil).

B. Javidi is with the Department of Electrical and Computer Engineering at University of Connecticut, Storrs, CT 06269-4157 USA (e-mail: Bahram.Javidi@UConn.edu).

Color versions of one or more of the figures are available online at http://ieeexplore.ieee.org.

Digital Object Identifier 10.1109/JDT.2013.2246857

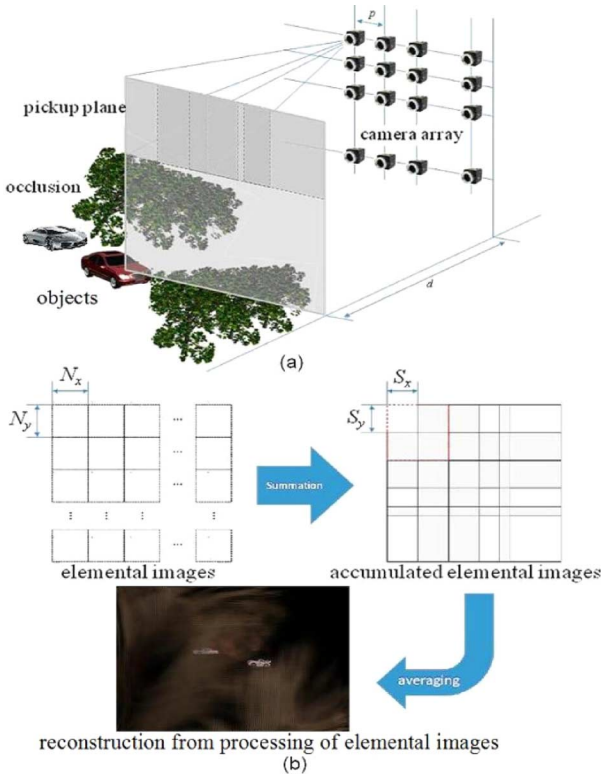

Fig. 2. 3D integral imaging sensing and reconstruction. (a) Scene capture process. (b) 3D reconstruction of the scene.

each perspective image on a full size imaging sensor [3], [19], [20]. Since the size of such an array quickly becomes a major concern, a single high resolution 2D image sensor can alternatively scan the aperture and capture intermittent images over a large area. This approach is known as synthetic aperture integral imaging (SAII) and overcomes some of the limitations of traditional lenslet-based integral imaging systems.

As illustrated in Fig. 2(a), a camera array or moving single camera is used to acquire the elemental images from slightly different perspectives. 3D images can be reconstructed by a variety of computational reconstruction algorithms [1], [3], [19]. Our procedure of computational reconstruction is shown in Fig. 2(b). Each elemental image is projected on the desired reconstruction plane and overlaps with all other back-projected elemental images. The computational reconstruction algorithm is

$$R(x,y,z) = \frac{1}{O(x,y)} \sum_{k=0}^{K-1} \sum_{l=0}^{L-1} E_{kl}\left(x - k\frac{N_x \times p}{c_x \times M}, y - l\frac{N_y \times p}{c_y \times M}\right) \quad (1)$$

where $R(x,y,z)$ represents the intensity of the reconstructed 3D image at depth $z = d$, x and y are the index of pixels, E_{kl} represents the intensity of the kth column and lth row elemental image, N_x, N_y are the total number of pixels for each elemental image, M is the magnification factor and equals z/f, f is the focal length, p is the pitch between image sensors, c_x, c_y are the size of the image sensor, $O(x,y)$ is the overlapping number matrix.

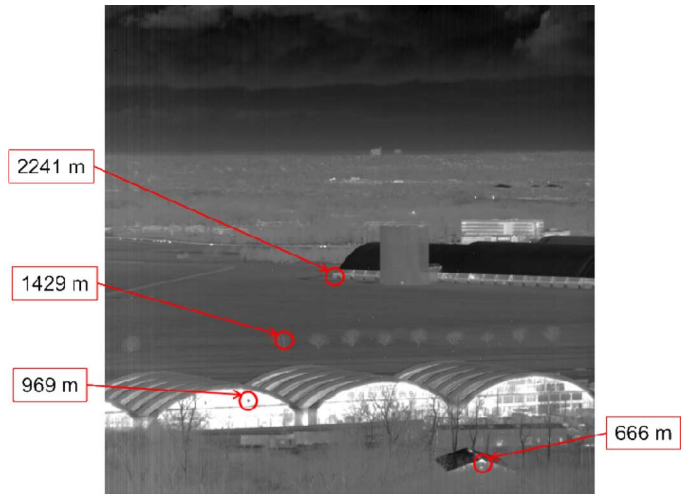

Fig. 3. Example of elemental image with range annotations.

Fig. 4. Tests were conducted from the Sensors Directorate tower and camera rail.

III. Field Collection

Field experiments were conducted from the 12th floor of the AFRL tower located at Wright Patterson AFB. All elemental images were collected with a Lockheed Martin Santa Barbara Focalplane AuraSR MWIR imager with a StingRay Optics 120 mm $f/2.3$ lens. This lens provides very low distortion over its $9.51° \times 9.51°$ field-of-view.

A representative elemental image is shown in Fig. 3. This west-facing view includes a historical hangar complex with flight line and the National Museum of the United States Air Force. The figure is annotated with measured ranges for a number of prominent objects in the scene. Range measurements were made with a Riegl Lasertape FG21 laser range finder. In each case, the most reliable measurements came from ranging the tower from the target. The importance of this distinction will become clear when these ranges are used to compare results later in Section IV.

Knowledge of camera position and orientation in the pickup stage of integral imaging is critical to all subsequent reconstruction tasks. For this reason, the AuraSR camera was translated between imaging positions using a high accuracy rail apparatus originally designed for synthetic aperture radar experiments (see Fig. 4). Camera position on the rail can be tightly controlled over a 9 m horizontal path resulting in only minor residual position and pointing errors. Fig. 5 shows these residual

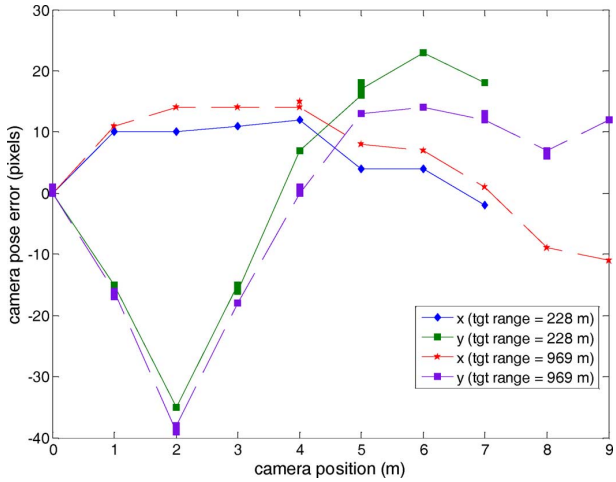

Fig. 5. Estimated residual camera positioning errors for two independent tests. "tgt" denotes target.

errors as estimated from known target ranges in two independent sets of elemental images.

This correction was used for fine camera position adjustments in the results that are shown below. It should be emphasized that the correction does not represent some target specific tuning of the results; a single set of translation correction parameters was used throughout each experiment to good effect. The interested reader may also refer to [21] for an alternative camera positioning correction method that does not require a reference target.

IV. Experiment 1—Imaging Through Obscurations

This first experiment demonstrates the use of computational integral imaging (CII) for profilimetry and, more importantly, imaging through obscurations. The independently measured sensor-to-target range is 228 m. To the best of our knowledge, this is the longest range demonstration of integral imaging for obscuration penetration available in the literature.

A complete explanation of CII reconstruction can be found in [3]. For the one-dimensional pick-up array used in these experiments, the image in the reconstruction plane at range z is given by

$$R(x,y,z) = \frac{1}{O(x,y,z)} \sum_{i=1}^{N} E_i\left(x - \frac{fp}{zD} + m_i, y + n_i\right) \tag{2}$$

where E_i is the ith elemental image out of N total images, f is the camera focal length, D is the camera pixel pitch, p is the separation distance between image sensors, and (m_i, n_i) are the fine position correction adjustments discussed in Section III. Both (x, y) and (m_i, n_i) are addressed in image pixel coordinates. O is the overlapping image number matrix, e.g., if three elemental images overlap at point (x, y, z) then $O(x, y, z) = 3$. Equation (2) should be interpreted as a horizontal sliding and summing of the elemental images according to their relative perspectives of the scene at range z. Visually, the effect of R is that targets in or near the reconstruction plane are sharply defined while those at different ranges are blurred out. Note that this blurring has nothing to do with camera focus. Focus is held constant across all elemental images.

Fig. 6. Obscured target as seen in an elemental image.

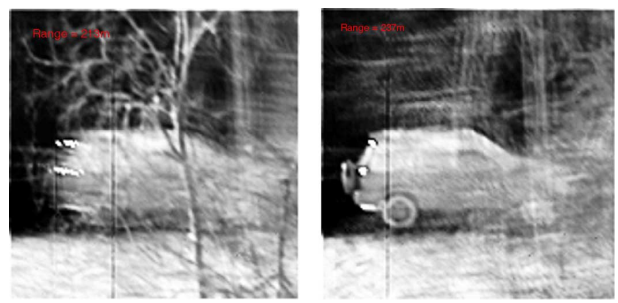

Fig. 7. Results of the obscuration penetration experiment.

Equation (2) is applied to the problem of obscuration penetration in the following scenario. The camera parameters are focal length $f = 120$ mm, and pixel size $= 19.5$ μm. The horizontal and vertical position correction factors are as shown in Fig. 5. As shown in Fig. 6, a civilian vehicle is partially obscured in a tree line. This image is also one of the $N = 8$ elemental images used in the CII reconstruction. It should be clear that much of the detail on this vehicle cannot be recovered from a single elemental image alone. The same is true for the remaining elemental images spread out over a horizontal pick-up range of 7 m. The full pick-up range could not be used due to field-of-view limitations.

The obscuration penetration effect is shown by reconstructing this scene at two ranges. Fig. 7 shows the trees in front of the vehicle reconstructed at a range of $z = 213$ m and the vehicle reconstructed at a range of $z = 237$ m.

The vehicle reconstruction is in a plane 9 m deeper than the ground truth sensor-to-target range. This difference could be due to errors in either the reconstruction or uncertainty in the ground truth measurements, but another interesting possibility exists as well. The decision to use a 237 m target reconstruction range was based on the visual appearance of the target. It may be that this reconstruction is most appealing because the foreground trees are extensively blurred out at this range, not because the target is in sharp relief. This hypothesis may be tested through future measurements involving more elemental images including vertical and horizontal camera positions.

The CII code used in the experiment was implemented in MATLAB. Total runtime for full scene reconstruction at any given range is 0.28 s. This is adequate for the present purposes

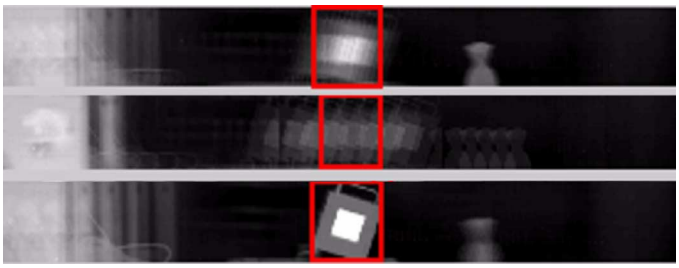

Fig. 8. Graphical representation of the CII search procedure at three ranges.

but more efficient implementations are possible and inspection of (2) shows that this process is easily parallelizable for additional speed gains.

V. Experiment 2—Range Estimation and 3-D Scene Reconstruction

The second goal of this research is to test the range estimation capability of computational integral imaging. All camera parameters are the same as in Experiment 1 except for the overall camera depression angle. While it is possible for a sensor operator to estimate range visually using CII, this estimate would be somewhat subjective. Instead, we implemented a procedure to automatically search for a reference template of each target in CII 3D space. The template data is taken from the (arbitrarily selected) reference elemental image and the search function is defined in terms of the sum squared error between the template image and like-sized image chips from $R(x, y, z)$ as defined in (1).

The geometry of the reconstruction algorithm allows for strong spatial constraints to be placed on the required reconstruction region and on the search function. For this particular experimental setup, there is no (intentional) motion in the y, i.e., vertical, direction. Consequently, the contributions of $R(x, y, z)$ outside of the template chip in the y-direction may be ignored. Implementing this constraint speeds up the range estimation algorithm significantly. Additionally, the projected location of the template image at a given range may be calculated in advance, thereby restricting the search to a specific region in the reconstruction plane. The location of this region will change at each range but this change is deterministic. This second constraint also speeds up the algorithm but, more importantly, it eliminates local minima in the search space that can stall otherwise applicable search algorithms. By identifying and applying these strong constraints, we were able to use $\mathrm{fminbnd}$ (a canned minimization function in MATLAB) to find the estimated range, z', with minimum sum squared error between the template, $T(x, y)$, and constrained CII reconstructed image, $Rc(x, y, z)$

$$z' = \arg\min_{z} \left\{ \sum_{x} \sum_{y} \left[T(x, y) - R_c(x, y, z) \right]^2 \right\}. \quad (3)$$

The search algorithm and constraints are demonstrated graphically in Fig. 8 using a laboratory CII dataset and three reconstructed ranges (top—range undershoot; middle—range overshoot; bottom—correct range). The y-direction constraint is implemented as a simple crop of the image along rows that are not consistent with the template chip. The template chip, in this case, contains the image of a tilted 2" blackbody source. The second constraint is shown as the red box over the CII image at each range. The spatial attributes of this red box change with each estimated range but this change is predictable because the position of the template chip in its reference elemental image is known. Only the sum squared error inside of the red box boundary is considered in the range estimation problem.

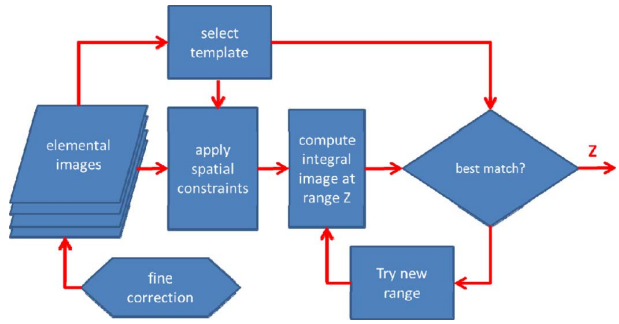

Fig. 9. Overview of the range search algorithm.

TABLE I
Estimated Range Results Using CII

Measured (m)	Estimated(m)	Δ (m)	MLR (m)
666	710	-44	8
969	1015	-46	17
1429	1443	-14	37
2241	2065	176	91

In integral imaging, longitudinal resolution depends on many system parameters including detector size, total parallax, focal length, and so on. Minimum longitudinal resolution (MLR) is typically defined in terms of a minimum z distance such that all the elemental images are focused on the same plane and not overlapped [25]. However, when $z \gg p_{\max}$ (where $p_{\max}$ is the parallax or the largest possible separation between elemental images) the elemental images always have significant overlap. Assuming detector limited (i.e., undersampled) imaging conditions; a useful estimate of MLR in this case is

$$\Delta z \geq \frac{dz^2}{f p_{\max}} \quad (4)$$

which is based on the requirements that a one pixel shift between elemental images is necessary to detect a change in depth and that $z \gg f$. The longitudinal resolution can be improved by increasing the parallax and/or reducing the pixel size. Also, it depends on the camera geometry. The limitation of the integral imaging in terms of resolution, parallax, and camera parameters are presented in [24] and [25]. While there are active sensing approaches such as LADAR that can measure range, the integral imaging approach presented here has the advantages of simplicity and passive sensing. [26] discusses both LADAR approach and integral imaging for ranging. MRL values are presented below to provide a reference by which the estimated range errors can be compared.

An overview of our search algorithm is shown in Fig. 9. Results using this search algorithm for four targets at known ranges are shown in Table I. Total processing time was 1.25 s (0.312

s per target) using non-optimized code. The Δ values shown in the table represent the difference between the laser rangefinder measured target range and the CII estimated range. In this way, a negative Δ value indicates that the target range was overestimated. MLR is, by definition, unsigned.

The resulting range errors are comparable to the MLR though clearly there is room for improvement. There are several possible reasons why the MLR was not achieved. First and most important, there may be pointing error that is not well modeled by the fine position correction adjustments [see eq. (1)] and/or there may be random error in the estimation of the adjustments themselves. Second, the imagery is undersampled and therefore each elemental image is not an exact translated replica of the others. Consequently, the objective function in (3) might be minimized at the wrong z due to aliasing along a sharp edge or other high contrast feature. Noise does not appear to be a contributing factor in this case though perhaps it would be under low signal conditions.

In several cases, this performance is better than what can be achieved with a laser rangefinder because of environmental conditions and target geometry. Our experience collecting ground truth for this project with a Riegl Lasertape FG21 laser rangefinder supports this claim. When viewed from the tower, the trees in front of the roof (bottom right) reflect more laser energy than the roof itself. Attempts to range this roof from the tower yielded results that were short by several hundred meters. The tree at true range 1429 m is also not a well formed target for a laser rangefinder for similar reasons. This is why the measured ranges shown in Section III were taken by ranging the tower from the target location: the tower is angularly larger and relatively unobstructed from or nearby each target site.

The target templates in these range estimation tests were hand selected but adequate results can also be achieved with an automatic image segmentation algorithm. Segmenting a grayscale image with many touching objects is another worthy research topic in and of itself. We used marker-controlled watershed segmentation[1] in order to test our CII ranging algorithm but there are many other viable approaches. Segmentation algorithm runtime was 3.6 s.

Each of these segments was ranged using the algorithm described above. The resulting range map is shown in Fig. 10. Total runtime was 59.00 s. While the overall results are good, two prominent segment types defeated the ranging algorithm: tree segments and periodic structure segments. Clumps of trees, especially those near the bottom of the image, may be difficult for the ranging algorithm because each segment contains significant 3D content. If this conjecture is true, then further segmentation (or perhaps more intelligent segmentation) may reduce these errors. Additionally, the low contrast and periodic structure of the museum hanger roof (near the upper right of the image) may have caused the search algorithm to fail by providing multiple matches to the segment. Assuming this is the case, a combination of vertically and horizontally dispersed elemental images may help clear up this ambiguity.

Qualitatively, it is easier to assess this range map using 3D projection as shown in Fig. 11. Most of the anomalous segments have been blacked out to maintain perspective. Several small remaining range anomalies are present, especially in the left half of the image. The museum hanger roof is also conspicuously missing for the reasons described above. Otherwise, the quality of the projection is surprisingly good.

[1][Online]. Available: http://www.mathworks.com/products/image/demos.html?file=/products/demos/shipping/images/ipexwatershed.html

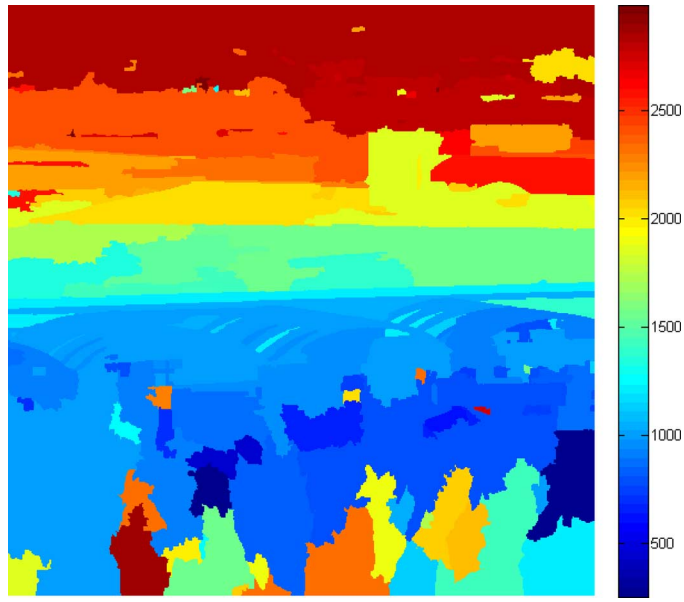

Fig. 10. Range map using automatic segmentation.

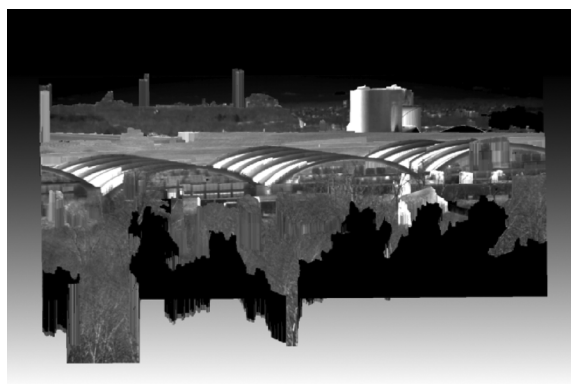

Fig. 11. Scene projection from computational integral imaging.

The interested reader may also refer to [22] for a completely unrelated alternative for range mapping using integral imaging. In this work, the authors demonstrate their approach using 121 elemental images with 5 mm spacing for targets with ranges out to 52 cm. We leave it to future work to determine if their approach can be translated to the sparse sampling, long range scenario presented here.

VI. Conclusion

In this paper, we describe our experiments in obscuration penetration and ranging using passive computational integral imaging (CII) at distances that greatly exceed anything published previously. The two key requirements for successful CII are control over camera pose and the ability to measure or estimate the relative change in camera position between elemental images. We were able to build elemental image arrays of up

to 9 m by employing rail guided positioning and fine corrections estimated from the target scene. In doing so, we were able to successfully perform obscuration penetration imaging from over 200 m and passive ranging at over 2000 m. To the best of our knowledge, these are by far the longest range examples of this technique available in the literature (see for instance, [21] and [22] for more typical ranges). In order to achieve these results, we also devised an automatic ranging algorithm based on fast 3-D template matching. In future research, this approach will be compared to other processing options in terms of speed and accuracy.

ACKNOWLEDGMENT

The authors would like to thank Lt. R. Hoggard (AFRL/RYMR) for rail access, repairs, and operational guidance. Thanks also to Mr. J. Servites (AFRL/RYMT) for access to tools, equipment, and advice from the Optical eXploitation (OX) Lab.

REFERENCES

[1] B. Javidi, F. Okano, and J.-Y. Son, *Three-Dimensional Imaging, Visualization, and Display Technologies*. New York, NY, USA: Springer Verlag, 2008.
[2] C. B. Burckhardt, "Optimum parameters and resolution limitation of integral photography," *J. Opt. Soc. Amer.*, vol. 58, pp. 71–76, 1968.
[3] A. Stern and B. Javidi, "Three-dimensional image sensing, visualization, and processing using integral imaging," *Proc. IEEE*, vol. 94, no. 3, pp. 591–607, Mar. 2006.
[4] F. Okano, J. Arai, K. Mitani, and M. Okui, "Real-time integral imaging based on extremely high resolution video system," *Proc. IEEE*, vol. 94, no. 3, pp. 490–501, Mar. 2006.
[5] R. Martinez-Cuenca, G. Saavedra, M. Martinez-Corral, and B. Javidi, "Progress in 3D multiperspective display by integral imaging," *Proc. IEEE*, vol. 97, no. 6, pp. 1067–1077, Jun. 2009.
[6] T. Okoshi, *Three-Dimensional Imaging Techniques*. New York, NY, USA: Academic, 1976.
[7] G. Lippmann, "La photographie integrale," *Comptes-Rendus Academie des Sciences*, vol. 146, pp. 446–451, 1908.
[8] J. Arai, F. Okano, H. Hoshino, and I. Yuyama, "Gradient index lens array method based on real time integral photography for three dimensional images," *Appl. Opt.*, vol. 37, pp. 2034–2045, 1998.
[9] L. Yang, M. McCornick, and N. Davies, "Discussion of the optics of a new 3-D imaging system," *Appl. Opt.*, vol. 27, pp. 4529–4534, 1988.
[10] F. Okano, H. Hoshino, J. Arai, and I. Yuyama, "Real-time pickup method for a three-dimensional image based on integral photography," *Appl. Opt.*, vol. 36, pp. 1598–1603, 1997.
[11] B. Lee, S. Jung, and J.-H. Park, "Viewing-angle-enhanced integral imaging using lens switching," *Opt. Lett.*, vol. 27, pp. 818–820, May 2002.
[12] M. Martinez-Corral, B. Javidi, R. Martinez-Cuenca, and G. Saavedra, "Integral imaging with improved depth of field by use of amplitude modulated microlens array," *Appl. Opt.*, vol. 43, pp. 5806–5813, Nov. 2004.
[13] J.-S. Jang, F. Jin, and B. Javidi, "Three-dimensional integral imaging with large depth of focus by use of real and virtual image fields," *Opt. Lett.*, vol. 28, pp. 1421–1423, 2003.
[14] B. Javidi, I. Moon, and S. Yeom, "Three-dimensional identification of biological microorganism using integral imaging," *Opt. Exp.*, vol. 14, pp. 12095–12107, 2006.
[15] B. Tavakoli, B. Javidi, and E. Watson, "Three dimensional visualization by photon counting computational integral imaging," *Opt. Exp.*, vol. 16, pp. 4426–4436, 2008.
[16] R. Schulein and B. Javidi, "Underwater multiview three-dimensional imaging," *J. Display Technol.*, vol. 4, no. 4, pp. 351–353, Dec. 2008.
[17] J.-S. Jang and B. Javidi, "Three-dimensional integral imaging of micro-objects," *Opt. Lett.*, vol. 29, pp. 1230–1232, 2004.
[18] B. Javidi and Y. S. Hwang, "Passive near-infrared 3D sensing and computational reconstruction with synthetic aperture integral imaging," *J. Display Technol.*, vol. 4, no. 1, pp. 3–5, Mar. 2008.
[19] A. Stern and B. Javidi, "3-D computational synthetic aperture integral imaging (COMPSAII)," *J. Opt. Express* Sep. 2003 [Online]. Available: http://www.opticsinfobase.org/oe/abstract.cfm?URI=oe-11-19-2446
[20] J. S. Jang and B. Javidi, "Three dimensional synthetic aperture integral imaging," *J. Opt. Lett.*, vol. 27, no. 13, pp. 1144–1146, Jul. 2002.
[21] X. Xiao, M. DaneshPanah, M. Cho, and B. Javidi, "3D integral imaging using sparse sensors with unknown positions," *J. Display Technol.*, vol. 6, no. 12, pp. 614–619, Dec. 2010.
[22] M. DaneshPanah and B. Javidi, "Profilometry and optical slicing by passive three-dimensional imaging," *Opt. Lett.*, vol. 34, pp. 1105–1107, 2009.
[23] S. Manolache, A. Aggoun, M. McCormick, N. Davies, and S. Y. Kung, "\Analytical model of a three-dimensional integral image recording system that uses circular- and hexagonal-based spherical surface microlenses," *J. Opt. Soc. Amer. A*, vol. 18, p. 1814, 2001.
[24] D. Shin, M. Daneshpanah, and B. Javidi, "Generalization of three-dimensional N-ocular imaging systems under fixed resource constraints," *Opt. Lett.*, vol. 37, pp. 19–21, 2012.
[25] D. H. Shin and B. Javidi, "Resolution analysis of N-ocular imaging systems with tilted image sensors," *J. Display Technol.*, vol. 8, no. 10, pp. 529–533, Oct. 2012.
[26] P. F. McManamon, B. Javidi, E. A. Watson, M. Daneshpanah, and R. Schulein, "New paradigms for active and passive 3D remote object sensing, visualization, and recognition," in *Proc. SPIE*, 2008, vol. 6967.

Daniel A. LeMaster received the B.S. degree in engineering physics from Wright State University, Dayton, OH, USA, and the M.S. degree in applied physics, and the Ph.D. degree in electrical engineering from the Air Force Institute of Technology, Wright Patterson AFB, OH, USA.

He is currently an EO/IR systems engineer at the Air Force Research Laboratory at Wright Patterson AFB, OH, USA, and has previously held positions in civil service, industry, and the U.S. Army. He is the author or co-author of 20 publications spread across journal and conference articles. His primary research interests include standoff reconnaissance imaging systems and polarimetric imaging.

Barry Karch received the B.S. degree in electrical engineering, the M.S. degree in electro-optics, and the M.S. degree in electrical engineering from the University of Dayton, Dayton OH, where he is currently pursuing the Ph.D. degree in electrical engineering.

He is currently a principal research electronics engineer in the Multispectral Sensing & Detection Division of the Air Force Research Laboratory, Wright-Patterson AFB OH, USA. He has worked in the areas of EO/IR remote sensor system and processing development for 25 years and his current research interests are in the areas of hyperspectral and polarimetric sensor development and exploitation.

Bahram Javidi (S'82–M'83–SM'96–F'98) received the B.S. degree from George Washington University, Washington, DC, USA, and the M.S. and Ph.D. degrees from the Pennsylvania State University, University Park, PA, USA, all in electrical engineering.

He is the Board of Trustees Distinguished Professor at the University of Connecticut. He has over 760 publications, including over 340 peer reviewed journal article, over 360 conference proceedings, including over 110 Plenary Addresses, Keynote Addresses, and invited conference papers. His papers have been cited over 10500 times according to the citation index of *WEB of Knowledge* ($h\text{-}index = 55$). He is a co author on nine best paper awards.

Dr. Javidi is Fellow of seven national and international professional scientific societies, including American Institute for Medical and Biological Engineering (AIMBE), Optical Society of America (OSA), and SPIE. In 2010, he was the recipient of The George Washington University's Distinguished Alumni Scholar Award, University's highest honor for its alumni in all disciplines. In 2008, he received a Fellow award by John Simon Guggenheim Foundation. He received the 2008 IEEE Donald G. Fink prized paper award among all (over 130) IEEE Transactions, Journals, and Magazines. In 2007, The Alexander von Humboldt Foundation awarded him with Humboldt Prize for outstanding U.S. scientists. He received the Technology Achievement Award from the International Society for Optical Engineering (SPIE) in 2008. In 2005, he received the Dennis Gabor Award in Diffractive Wave Technologies from the SPIE. Early in his career, the National Science Foundation named him a Presidential Young Investigator and he received The Engineering Foundation and the Institute of Electrical and Electronics Engineers (IEEE) Faculty Initiation Award. He was selected in 2003 as one of the nation's top 160 engineers between the ages of 30–45 by the National Academy of Engineering (NAE) to be an invited speaker at The Frontiers of Engineering Conference. He is on the Editorial Board of the Proceedings of the IEEE Journal (ranked #1 among all electrical engineering journals), and he was on the founding board of editors of IEEE/OSA JOURNAL OF DISPLAY TECHNOLOGY.